Inorganic Chemistry
Article

Inorg. Chem. **2011**, *50*, 1633–1647 **1633**
DOI: 10.1021/ic101832c

Reactions of Copper(II)-Phenol Systems with O_2: Models for TPQ Biosynthesis in Copper Amine Oxidases

Kae Tabuchi,[†] Mehmed Z. Ertem,[‡] Hideki Sugimoto,[†] Atsushi Kunishita,[†] Tetsuro Tano,[†] Nobutaka Fujieda,[†] Christopher J. Cramer,*[,‡] and Shinobu Itoh*[,†]

[†]*Department of Material and Life Science, Division of Advanced Science and Biotechnology, Graduate School of Engineering, Osaka University, 2-1 Yamada-oka, Suita, Osaka 565-0871, Japan, and* [‡]*Department of Chemistry and Supercomputing Institute, University of Minnesota, 207 Pleasant St. SE, Minneapolis, Minnesota 55455, United States*

Received September 7, 2010

Copper(II) complexes supported by a series of phenol-containing bis(pyridin-2-ylmethyl)amine N_3 ligands (denoted as **L^{o}H**, **L^{m}H**, and **L^{p}H**) have been synthesized, and their O_2 reactivity has been examined in detail to gain mechanistic insights into the biosynthesis of the TPQ cofactor (2,4,5-trihydroxyphenylalaninequinone, TOPA quinone) in copper-containing amine oxidases. The copper(II) complex of **L^{o}H** (*ortho*-phenol derivative) involves a direct phenolate to copper(II) coordination and exhibits almost no reactivity toward O_2 at 60 °C in CH_3OH. On the other hand, the copper(II) complex of **L^{m}H** (*meta*-phenol derivative), which does not involve direct coordinative interaction between the phenol moiety and the copper(II) ion, reacts with O_2 in the presence of triethylamine as a base to give a methoxy-substituted *para*-quinone derivative under the same conditions. The product structure has been established by detailed nuclear magnetic resonance (NMR), infrared (IR) spectroscopy, and electrospray ionization−mass spectroscopy (ESI-MS) (including ^{18}O-labeling experiment) analyses. Density functional theory predicts that the reaction involves (i) intramolecular electron transfer from the deprotonated phenol (phenolate) to copper(II) to generate a copper(I)-phenoxyl radical; (ii) the addition of O_2 to this intermediate, resulting in an end-on copper(II) superoxide; (iii) electrophilic substitution of the phenolic radical to give a copper(II)-alkylperoxo intermediate; (iv) O−O bond cleavage concomitant with a proton migration, giving a *para*-quinone derivative; and (v) Michael addition of methoxide from copper(II) to the *para*-quinone ring and subsequent O_2 oxidation. This reaction sequence is similar to that proposed for the biosynthetic pathway leading to the TPQ cofactor in the enzymatic system. The generated *para*-quinone derivative can act as a turnover catalyst for aerobic oxidation of benzylamine to *N*-benzylidene benzylamine. Another type of copper(II)-phenol complex with an **L^{p}H** ligand (*para*-phenol derivative) also reacts with O_2 under the same experimental conditions. However, the product of this reaction is a keto-alcohol derivative, the structure of which is qualitatively different from that of the cofactor. These results unambiguously demonstrate that the steric relationship between the phenol moiety and the supported copper(II) ion is decisive in the conversion of active-site tyrosine residues to the TPQ cofactor.

Introduction

Redox reactions between copper(II) ions and the phenol groups of tyrosines in enzyme active sites are involved in the biogenetic production of novel organic cofactors such as TPQ (2,4,5-trihydroxyphenylalaninequinone, TOPA quinone) by copper-containing amine oxidases, LTQ (lysine tyrosylquinone) by lysyl oxidase, and Tyr-Cys by galactose oxidase (see Figure 1).[1] All of these cofactors are derived from encoded tyrosine residues (with their phenol groups) placed near the mononuclear copper reaction sites; the post-translational modification reactions proceed spontaneously with the addition of the copper ion and O_2 to the apo-enzymes, i.e., without the intermediacy of any external enzymes (so-called "self-processing").

As an example, the TPQ cofactor of copper-containing amine oxidases has been demonstrated to be generated by self-processing of the active site tyrosine (Tyr), a potential mechanism for which is illustrated in Scheme 1.[1a,b,e,g,h,j,2] In particular, interaction of the phenolate oxygen (deprotonated form) of Tyr with the copper(II) ion in the holo-enzyme **A** may induce electron transfer from the phenolate to copper(II), generating a phenoxyl radical−copper(I) intermediate (**B**), to which molecular oxygen (O_2) may then be added. In this process, the O_2 moiety is formally reduced by two electrons—one from copper(I) and the other from the phenoxyl

*Author to whom correspondence should be addressed. E-mail: shinobu@mls.eng.osaka-u.ac.jp (S.I.), cramer@umn.edu (C.J.C.).

Published on Web 02/01/2011

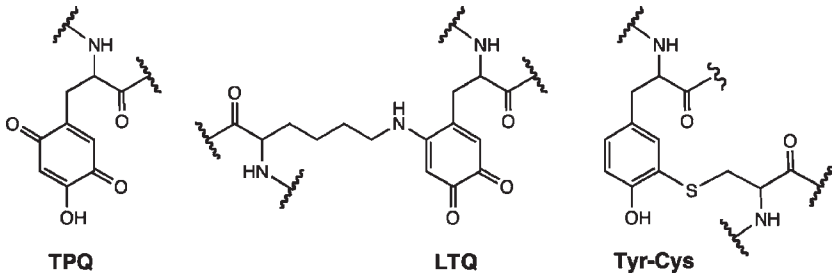

Figure 1. Organic cofactors of amine oxidase (TPQ), lysyl oxidase (LTQ), and galactose oxidase (Tyr-Cys) post-translationally derived from an active-site tyrosine.

radical moiety—to produce a copper(II)-alkylperoxo-type intermediate (**C**). Subsequent heterolytic cleavage of the O−O bond in **C** can occur to give the copper(II)-hydroxo *o*-quinone species **D**, and following Michael addition of the generated hydroxide to the 5-position of the *o*-quinone intermediate **D′** gives the reduced TPQ cofactor TPQ_{red}. Aerobic oxidation of TPQ_{red} is the last step required to produce TPQ_{ox}. Similar mechanisms may be inferred for the biosynthesis of the LTQ cofactor of lysyl oxidase, where Michael addition of a nearby lysine residue occurs instead of the addition of hydroxide to the *o*-quinone intermediate. To date, the hydroxide addition step of TPQ biosynthesis (**D′** → TPQ) has been investigated in model systems,[3] but little has been explored for the initial aerobic oxidation process of Tyr catalyzed by the copper(II) ion (Tyr → **D**).

In this study, we examine the reactions of mononuclear copper(II) complexes supported by a series of bis(pyridin-2-ylmethyl)amine ligands that have a phenol group attached to the 6-position of one of the pyridine donor groups (L^oH, L^mH, and L^pH; see Chart 1) when exposed to molecular oxygen. The ligands are designed to mimic the reaction center of the apo-form of copper-containing amine oxidases (see Figure 2), where three histidine imidazole ligands and a tyrosine residue (the precursor of TPQ cofactor) are present. To examine the effect on the biosynthetic process of different Tyr phenol geometries, relative to the copper ion, three types of phenol-containing ligands—$\mathbf{L^oH}$, $\mathbf{L^mH}$, and $\mathbf{L^pH}$—have been designed. In the case of $\mathbf{L^oH}$, direct coordination of the phenolate oxygen to the bound metal ion will occur, whereas such a coordinative interaction is unlikely to be involved in the $\mathbf{L^mH}$ and $\mathbf{L^pH}$ ligand systems. On the basis of product analyses and theoretical calculations, mechanistic aspects of the post-translational modification of Tyr to the TPQ cofactor are discussed.

Experimental Section

General. Reagents and solvents used in this study, except the ligands and complexes, were commercial products of the highest available purity and were further purified by standard methods, if necessary.[5] *N*-(6-Phenylpyridin-2-yl)methylbenzylamine (**1**), 6-(3-methoxyphenyl)pyridin-2-ylcarboxyaldehyde ($\mathbf{2^m}$), and 6-(4-methoxyphenyl)pyridin-2-ylcarboxyaldehyde ($\mathbf{2^p}$) were prepared according to reported methods.[6] $[Cu^{II}(L^o)](ClO_4)$ ($\mathbf{Cu^{II}L^o}$) was prepared as described in a previous study.[7] Fourier transform infrared (FT-IR) spectra were recorded using a Shimadzu Model FTIR-8200PC system. Mass spectra were recorded using a JEOL Model JMS−700T Tandem MS station or a JEOL Model JMS−700 apparatus. NMR spectra were recorded using various equipment (JEOL Model LMN−ECP300WB, JEOL Model ECP400, JEOL Model ECS400, or Varian Model UNITY INOVA 600 MHz). ELectron spin resonance (ESR) measurements were performed on a Bruker Model E-500 spectrometer at −150 °C, using a variable-temperature cell holder or a JEOL Model JES-FA100 apparatus. Anaerobic reactions were carried out after bubbling argon gas gently through a thin syringe needle for ∼30 min to a solution in a reaction vessel or in an ultraviolet−visible light (UV−vis) cell, which was tightly closed by a silicon rubber cap.

X-ray Structure Determination. Each single crystal was mounted on a glass fiber. X-ray diffraction (XRD) data were collected by a Rigaku Model RAXIS−RAPID imaging plate two-dimensional area detector, using graphite-monochromated Mo Kα radiation (λ = 0.71069 Å) to $2\theta_{max}$ of 55°. All of the crystallographic calculations were performed using the Crystal

(1) (a) Matsuzaki, R.; Suzuki, S.; Yamaguchi, K.; Fukui, T.; Tanizawa, K. *Biochemistry* **1995**, *34*, 4524–4530. (b) Tanizawa, K. *J. Biochem.* **1995**, *118*, 671–678. (c) Klinman, J. P. *J. Biol. Chem.* **1996**, *271*, 27189–27192. (d) McGuirl, M. A.; Dooley, D. M. *Curr. Opin. Chem. Biol.* **1999**, *3*, 138–144. (e) Dooley, D. M. *J. Biol. Inorg. Chem.* **1999**, *4*, 1–11. (f) Rogers, M. S.; Baron, A. J.; McPherson, M. J.; Knowles, P. F.; Dooley, D. M. *J. Am. Chem. Soc.* **2000**, *122*, 990–991. (g) Okeley, N. M.; van der Donk, W. A. *Chem. Biol.* **2000**, *7*, R159–R171. (h) Halcrow, M. A. *Angew. Chem., Int. Ed.* **2001**, *40*, 346–349. (i) Xie, L. L.; van der Donk, W. A. *Proc. Natl. Acad. Sci. U.S.A.* **2001**, *98*, 12863–12865. (j) Kim, M.; Okajima, T.; Kishishita, S.; Yoshimura, M.; Kawamori, A.; Tanizawa, K.; Yamaguchi, H. *Nat. Struct. Biol.* **2002**, *9*, 591–596. (k) Mure, M.; Mills, S. A.; Klinman, J. P. *Biochemistry* **2002**, *41*, 9269–9278. (l) Firbank, S. J.; Rogers, M.; Hurtado-Guerrero, R.; Dooley, D. M.; Halcrow, M. A.; Phillips, S. E. V.; Knowles, P. F.; McPherson, M. J. *Biochem. Soc. Trans.* **2003**, *31*, 506–509. (m) Rogers, M. S.; Dooley, D. M. *Curr. Opin. Chem. Biol.* **2003**, *7*, 189–196. (n) Whittaker, M. M.; Whittaker, J. W. *J. Biol. Chem.* **2003**, *278*, 22090–22101. (o) Whittaker, J. W. *Arch. Biochem. Biophys.* **2005**, *433*, 227–239. (p) Dominy, J. E.; Hwang, J.; Guo, S.; Hirschberger, L. L.; Zhang, S.; Stipanuk, M. H. *J. Biol. Chem.* **2008**, *283*, 12188–12201. (q) Rogers, M. S.; Hurtado-Guerrero, R.; Firbank, S. J.; Halcrow, M. A.; Dooley, D. M.; Phillips, S. E. V.; Knowles, P. F.; McPherson, M. J. *Biochemistry* **2008**, *47*, 10428–10439.

(2) (a) Schwartz, B.; Dove, J. E.; Klinman, J. P. *Biochemistry* **2000**, *39*, 3699–3707. (b) Dove, J. E.; Schwartz, B.; Williams, N. K.; Klinman, J. P. *Biochemistry* **2000**, *39*, 3690–3698. (c) Samuels, N. M.; Klinman, J. P. *J. Biol. Chem.* **2006**, *281*, 21114–21118. (d) DuBois, J. L.; Klinman, J. P. *Biochemistry* **2006**, *45*, 3178–3188. (e) Moore, R. H.; Spies, M. A.; Culpepper, M. B.; Murakawa, T.; Hirota, S.; Okajima, T.; Tanizawa, K.; Mure, M. *J. Am. Chem. Soc.* **2007**, *129*, 11524–11534.

(3) (a) Mure, M.; Tanizawa, K. *Biosci., Biotechnol., Biochem.* **1997**, *61*, 410–417. (b) Mandal, S.; Lee, Y.; Purdy, M. M.; Sayre, L. M. *J. Am. Chem. Soc.* **2000**, *122*, 3574–3584.

(4) Wilce, M. C. J.; Dooley, D. M.; Freeman, H. C.; Guss, J. M.; Matsunami, H.; McIntire, W. S.; Ruggiero, C. E.; Tanizawa, K.; Yamaguchi, H. *Biochemistry* **1997**, *36*, 16116–16133.

(5) Perrin, D. D.; Armarego, W. L. F.; Perrin, D. R. *Purification of Laboratory Chemicals*, 4th ed.; Pergamon Press: Elmsford, NY, 1996.

(6) (a) He, Z.; Craig, D. C.; Colbran, S. B. *J. Chem. Soc., Dalton Trans.* **2002**, 4224–4235. (b) Chuang, C.-l.; Lim, K.; Chen, Q.; Zubieta, J.; Canary, J. W. *Inorg. Chem.* **1995**, *34*, 2562–2568. (c) Jensen, M. P.; Lange, S. J.; Mehn, M. P.; Que, E. L.; Que, L. *J. Am. Chem. Soc.* **2003**, *125*, 2113–2128. (d) He, Z.; Colbran, S. B.; Craig, D. C. *Chem.—Eur. J.* **2003**, *9*, 116–129. (e) Tabuchi, K.; Sugimoto, H.; Kunishita, A.; Fujieda, N.; Itoh, S. *Inorg. Chem.* **2010**, *49*, 6820–6822.

(7) Kunishita, A.; Teraoka, J.; Scanlon, J. D.; Matsumoto, T.; Suzuki, M.; Cramer, C. J.; Itoh, S. *J. Am. Chem. Soc.* **2007**, *129*, 7248–7249.

Scheme 1

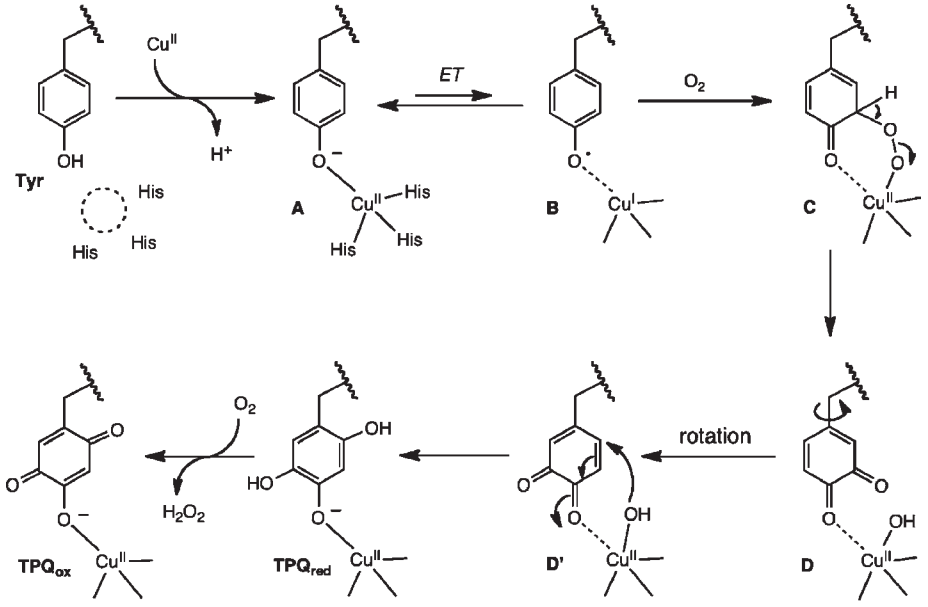

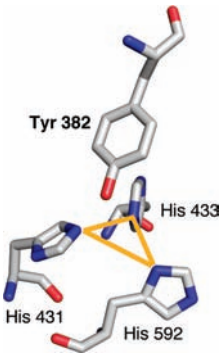

Figure 2. Active site of apo-form of copper-containing amine oxidase generated from PDB data (1AVK) using PyMol (DeLano Scientific LLC).[4]

Chart 1

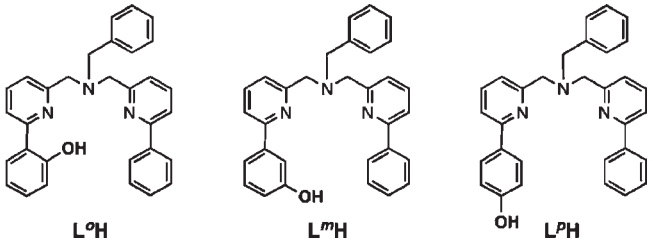

Structure software package of the Molecular Structure Corporation [Crystal Structure: Crystal Structure Analysis Package version 3.8.1, Molecular Structure Corp. and Rigaku Corp. (2005)]. The structures were solved using the SIR92 or SHELX97 programs and refined with CRYSTALS. All non-hydrogen atoms and hydrogen atoms were refined anisotropically and isotropically, respectively. Atomic coordinates, thermal parameters, and intramolecular bond distances and angles are provided in the Supporting Information (CIF file in a text format).

Ligand Synthesis. ***N*-[6-(3-Methoxyphenyl)pyridin-2-ylmethyl]-*N*-(6-phenylpyridin-2-ylmethyl)benzylamine (3^m).** Sodium cyanoborohydride (0.39 g, 6.21 mmol) was added slowly to a mixture of 6-(3-methoxyphenyl)pyridin-2-ylcarboxyaldehyde (**2^m**) (1.19 g, 5.24 mmol), *N*-(6-phenylpyridin-2-yl)methylbenzylamine (**1**) (1.42 g, 5.18 mmol), and acetic acid (0.33 mg, 5.49 mmol) in methanol (200 mL) with cooling, using a water−ice bath. The resulting mixture was stirred at room temperature for 3 days and then acidified by adding concentrated hydrochloric acid to quench the remaining sodium cyanoborohydride. The pH level of the solution was brought to 14 by adding concentrated sodium carbonate, and the resulting solution was evaporated under reduced pressure to remove methanol. The mixture was extracted with CH_2Cl_2 (50 mL × 3), and the combined organic layer was dried over Na_2SO_4. After removal of Na_2SO_4 by filtration, evaporation of the solvent afforded a yellowish oily material. Column chromatography on silica gel (hexane and ethyl acetate eluent) gave the titled compound **3^m** in 86% yield (2.1 g, 4.45 mmol). ^{1}H NMR (400 MHz, $CDCl_3$): δ 3.83 (2 H, s, $-CH_2-$), 3.89 (3 H, s, $-CH_3$), 3.98 (2 H, s, $-CH_2-$), 3.99 (2H, s, $-CH_2-$), 6.96 (1 H, ddd, J = 8.2 Hz, 2.6 and 0.9 Hz), 7.23−7.28 (1 H, m), 7.33−7.42 (4 H, m), 7.44−7.53 (4 H, m), 7.56−7.64 (6 H, m), 7.74 (2 H, td, J = 7.9 and 1.6 Hz), 8.02 (2 H, d, J = 7.3 Hz); HRMS (FAB$^+$): m/z = 472.2384. Calcd for $(C_{32}H_{30}N_3O)^+$ 472.2389.

***N*-[(6-(3-Hydroxylphenyl)pyridin-2-ylmethyl)-*N*-(6-phenylpyridin-2-ylmethyl)benzylamine (L^{m}H).** BBr_3 (5 mL of a 1.0 M CH_2Cl_2 solution) was added to compound **3^m** (1.5 g, 3.18 mmol) dissolved in CH_2Cl_2 (50 mL) in a three-neck round-bottom flask under a nitrogen atmosphere. The mixture was refluxed for 30 h under a nitrogen atmosphere. The final reaction mixture was then poured into methanol (50 mL), evaporated to dryness on a rotary evaporator, and three such cycles of addition of methanol and evaporation of solvent were performed to eliminate any volatile compounds. Finally, the yellowish oil was suspended in CH_2Cl_2 (30 mL), which was dissolved in methanol (20 mL) and water (20 mL). The pH of the solution was increased to 7, and at this pH level, a pale yellow compound was extracted with CH_2Cl_2 (50 mL × 3). The combined organic layer was dried over Na_2SO_4. After removal of Na_2SO_4 by filtration, evaporation of the solvent afforded a yellowish oily product. Column chromatography on silica gel (hexane and ethyl acetate eluent) gave the titled compound **L^{m}H** in 63% yield (0.92 g, 2.01 mmol,). ^{1}H NMR (300 MHz, $CDCl_3$): δ 3.77 (2 H, s, $-CH_2-$), 3.94 (2 H, s, $-CH_2-$), 3.99 (2 H, s, $-CH_2-$), 6.80 (1 H, ddd, J = 8.1 Hz, 2.7 Hz, and 0.9 Hz), 7.22−7.24 (1 H, m), 7.27−7.33 (2 H, m), 7.37−7.45 (7 H, m), 7.48−7.57 (5 H, m), 7.67−7.72 (2 H, m), 7.67−7.72 (2 H, m), 7.96 (2 H, d, J = 7.2 Hz); HRMS (FAB$^+$): m/z = 458.2235. Calcd for $(C_{31}H_{27}N_3O)^+$ 458.2232.

***N*-[6-(4-Methoxyphenyl)pyridin-2-ylmethyl]-*N*-(6-phenylpyridin-2-ylmethyl)benzylamine (3^p).** This compound was prepared in a similar manner for the synthesis of 3^m, using 6-(4-methoxyphenyl)pyridin-2-ylcarboxyaldehyde (2^p), instead of 2^m (70% isolated yield). ^{1}H NMR (400 MHz, $CDCl_3$): δ 3.82 (2 H, s, $-CH_2-$), 3.86 (3 H, s, -OCH_3), 3.95 (2 H, s, $-CH_2-$), 3.97 (2 H, s, $-CH_2-$), 6.98 (2 H, d, J = 8.8 Hz), 7.23−7.27 (1 H. m), 7.34 (2 H, t, J = 7.4 Hz), 7.41 (1 H, d, J = 7.2 Hz), 7.44−7.54 (6 H, m), 7.59 (2 H, t, J = 7.8 Hz), 7.68−7.76 (2 H, m), 7.97 (2 H, d, J = 8.8 Hz), 8.01 (2 H, d, J = 6.8 Hz); HRMS (FAB^+): m/z = 472.2385. Calcd for $(C_{32}H_{30}N_3O)^+$ 472.2389.

***N*-[(6-(3-Hydroxylphenyl)pyridin-2-ylmethyl)-*N*-(6-phenylpyridin-2-ylmethyl)benzylamine (L^pH).** This compound was prepared in a similar manner for the synthesis of L^mH, using 3^p instead of 3^m (41% isolated yield). ^{1}H NMR (400 MHz, $CDCl_3$): δ 3.79 (2 H, s, $-CH_2-$), 3.95 (2 H, s, $-CH_2-$), 3.97 (2 H, s, $-CH_2-$), 6.75 (2 H, d, J = 9.2), 7.23 (1 H, t, J = 7.4), 7.32 (2 H, t, J = 7.6 Hz), 7.52−7.39 (1 H, m), 7.42−7.48 (5 H, m), 7.52−7.59 (3 H, m), 7.66−7.40 (2 H, m), 7.78 (2 H, d, J = 9.2 Hz), 7.96 (2 H, d, J = 6.8 Hz); HRMS (FAB^+): m/z = 458.2220. Calcd for $(C_{31}H_{27}N_3O)^+$ 458.2232.

Synthesis of Copper(II) Complexes. $[Cu^{II}(L^mH)(CH_3CN)](ClO_4)_2$ ($Cu^{II}L^mH$). $Cu^{II}(ClO_4)_2\cdot 6H_2O$ (74 mg, 0.20 mmol) was added to an acetonitrile solution (5 mL) of ligand L^mH (92 mg, 0.20 mmol) and stirred for 15 min at room temperature. The addition of ether (100 mL) to the solution gave a green powder that was precipitated by allowing the mixture to stand for 30 min. The supernatant was then removed by decantation, and the remained green solid was washed with ether three times and dried to give complex $Cu^{II}L^mH$ in 75%. Single crystals of $Cu^{II}L^mH$ were obtained by vapor diffusion of ether into an acetone:CH_3CN (5:1) solution of the complex. FT-IR (KBr, cm^{-1}): 1114 and 623 (ClO_4^-), 3374 (OH); HRMS (FAB^+) m/z = 520.1445; Calcd for $C_{31}H_{27}N_3OCu$ 520.1450; Anal. Calcd for: $[Cu^{II}(L^m)(CH_3CN)](ClO_4)_2\cdot H_2O$: C, 50.87; H, 4.14; N, 7.19. Found: C, 50.71; H, 3.92; N, 7.00.

$[Cu^{II}(L^pH)(CH_3CN)](ClO_4)_2$ ($Cu^{II}L^pH$). This compound was synthesized by following the same procedure as that described for the preparation of $Cu^{II}L^mH$, using L^pH (92 mg, 0.20 mmol) instead of L^mH as a green powder in a 82% yield. Single crystals of $Cu^{II}L^pH$ were obtained by vapor diffusion of ether into an acetone:CH_3CN (5:1) solution of the complex. FT-IR (KBr, cm^{-1}): 1094 and 626 (ClO_4^-), 3371 (OH); HRMS (FAB^+) m/z = 520.1474; Calcd for $C_{31}H_{27}N_3Ocu$ 520.1450; Anal. Calcd for $[Cu^{II}(L^pH)(CH_3CN)](ClO_4)_2\cdot H_2O\cdot {}^1/_2CH_3CN$: C, 50.67; H, 4.05; N, 6.46. Found: C, 50.87; H, 4.24; N, 6.66.

$[Cu^{II}(4)(OCH_3)](ClO_4)$ ($Cu^{II}4$). $Cu^{II}L^mH$ (50 mg, 0.066 mmol) was dissolved in methanol (30 mL), and then Et_3N (2 equiv) was added to the solution. The resulting solution was stirred for 3 days at room temperature. After the reaction, the solvent was removed under reduced pressure to give a brown residue, to which ether (100 mL) was added. Brown powder was gradually precipitated by allowing the mixture to stand for several minutes. The supernatant was then removed by decantation, and the remaining brown solid was washed with ether three times and dried to give complex $Cu^{II}4$ in 94%. FT-IR (KBr, cm^{-1}): 1108 and 622 (ClO_4^-); HRMS (FAB^+) m/z = 595.1514; Calcd for $C_{33}H_{30}N_3O_4Cu$ 595.1532.

Isolation and Structure Determination of Modified Ligands 4 and 5H. After the reaction described above, the mixture was dissolved in CH_2Cl_2 (20 mL) and a 25% NH_3 aqueous solution (10 mL) was added to the solution. The aqueous solution was then extracted with CH_2Cl_2 (30 mL × 3), and the combined organic layer was dried over Na_2SO_4. After removal of Na_2SO_4 by filtration, evaporation of the solvent gave a brown material. The ^{1}H NMR spectrum of the resulting brown material indicated that compound **4** was produced in 51% (NMR yield based on $Cu^{II}L^mH$, using CH_2Br_2 as an internal standard). A SiO_2 column chromatographic treatment of the brown material (hexane and ethyl acetate eluent) converted some of compound **4** to compound **5H**. Thus, the isolated yield of **4** was 6% and that of **5H** was 25%, based on the starting copper(II) complex $Cu^{II}L^mH$ after the SiO_2 column chromatography.

4. ^{1}H NMR (400 MHz, $CDCl_3$): δ 3.71 (3 H, s, $-CH_3$), 3.77 (2 H, s, $-CH_2-$), 3.91 (2 H, s, $-CH_2-$), 3.91 (2 H, s, $-CH_2-$), 6.74 (1 H, d, J = 10.0 Hz), 6.77 (1 H. d, J = 10.4 Hz), 7.16 (1 H, dd, J = 7.4 and 1.6 Hz), 7.22−7.25 (1 H, m), 7.33 (2 H, t, J = 7.4 Hz), 7.39 (1 H, t, J = 7.2 Hz), 7.44−7.47 (4 H, m), 7.51 (1 H, d, J = 7.2 Hz), 7.59 (1 H, d, J = 7.6 Hz), 7.70−7.77 (3 H, m), 7.99 (2 H, d, J = 6.8 Hz); FT-IR (NaCl) 1672 and 1727 cm^{-1} (C=O); HRMS (FAB^+) m/z = 502.2159; Calcd for $C_{32}H_{28}N_3O_3^+$ 502.2131.

5H. ^{1}H NMR (400 MHz, $CDCl_3$): 3.89 (2 H, s, H_{23}), 3.96 (2 H, s, H_1), 4.03 (2 H, s, H_{13}), 6.71 (1 H, d, J = 10.2 Hz, H_{10}), 6.83 (1 H. d, J = 10.2 Hz, H_9), 7.00 (1 H, d, J = 7.6 Hz, H_3), 7.22−7.26 (1 H, m, H_{27}), 7.31 (2 H, t, J = 7.6 Hz, H_{26}), 7.39 (1 H, t, J = 7.2 Hz, H_{22}), 7.43−7.47 (2 H, m, H_{21}), 7.52 (2 H, d, J = 7.2 Hz, H_{25}), 7.56 (1 H, d, J = 7.6 Hz, H_{17}), 7.61 (1 H, d, J = 7.2 Hz, H_{15}), 7.71 (1 H, t, J = 7.6 Hz, H_{16}), 7.77 (2 H, t, J = 8.2 Hz, H_4), 7.94 (2 H, d, J = 7.2 Hz, H_{20}), 9.04 (1 H, d, J = 9.2 Hz, H_5); ^{13}C NMR (100 MHz, $CDCl_3$): 55.26 (C_{23}), 60.02 (C_1), 61.12 (C_{13}), 104.28 (C_7), 117.99 (C_3), 119.05 (C_{17}), 121.81 (C_5), 122.21 (C_{15}), 126.81 (C_{20}), 127.68 (C_{27}), 128.54 (C_{26}), 128.70 (C_{21}), 128.93 (C_{22}), 129.38 (C_{25}), 132.74 (C_9), 137.14 (C_{24}), 137.37 (C_{16}), 139.15 (C_{19}), 141.90 (C_4), 143.56 (C_{10}), 148.71 (C_2), 152.88 (C_6), 156.52 (C_{18}), 157.45 (C_{14}), 173.90 (C_{12}), 183.52 (C_8), 184.38 (C_{11}); FT-IR (NaCl, cm^{-1}) 1686 and 1731 (C=O), 3474 (OH); HRMS (FAB^+) m/z = 488.1990; Calcd for $C_{32}H_{28}N_3O_3^+$ 488.1974.

$[Cu^{II}(6)](ClO_4)$ ($Cu^{II}6$). $Cu^{II}L^pH$ (50 mg, 0.066 mmol) was dissolved in methanol (30 mL) and Et_3N (2 equiv) was added to the solution. The resulting solution was stirred for 3 days at 60 °C, and then the solvent was reduced under reduced pressure to give a brown residue. The addition of ether (100 mL) to the residue gave a brown powder, which precipitated by allowing the mixture to stand for several minutes. The supernatant was then removed by decantation, and the remaining brown solid was washed with ether three times and dried to give complex $Cu^{II}6$ in 80%. FT-IR (KBr, cm^{-1}): 1192 and 621 (ClO_4^-), 1665 (C=O); MS (ESI^+) m/z = 535.1; Calcd for $C_{31}H_{26}N_3O_2Cu$ 535.1.

Isolation and Structure Determination of Modified Ligand 6H. After the reaction described above, the reaction mixture was dissolved in CH_2Cl_2 (20 mL) and 25% NH_3 aqueous solution (10 mL) was added to the solution. The aqueous solution was then extracted with CH_2Cl_2 (30 mL × 3), and the combined organic layer was dried over Na_2SO_4. After the removal of Na_2SO_4 by filtration, evaporation of the solvent gave a brown material. The ^{1}H NMR spectrum of the resulting brown material indicated that compound **6H** was produced in 56% (NMR yield based on $Cu^{II}L^pH$ using CH_2Br_2 as an internal standard). ^{1}H NMR (400 MHz, $CDCl_3$): δ 3.79 (2 H, s, H_{21}), 3.93 (2 H, s, H_{11}), 3.94 (2 H, s, H_1), 6.26 (2 H, d, J = 8.8 Hz, H_8), 6.48 (1 H, s, OH_{26}), 6.72 (2 H. d, J = 8.8 Hz, H_9), 7.09 (1 H, d, J = 7.6 Hz, H_5), 7.26−7.31 (1 H, m, H_{25}), 7.36 (2 H, t, J = 8.4 Hz, H_{24}), 7.40−7.42 (1 H, m, H_{20}), 7.46 (2 H, d, J = 7.2 Hz, H_{23}), 7.49−7.54 (3 H, m, H_{13} and H_{19}), 7.59−7.64 (2 H, m, H_3 and H_{15}), 7.68 (1 H, t, J = 7.6 Hz, H_4), 7.74 (1 H, t, J = 7.8 Hz, H_{14}), 8.00 (2 H, d, J = 8.4 Hz, H_{18}); ^{13}C NMR (100 MHz, $CDCl_3$): 58.82 (C_{21}), 59.30 (C_1), 60.19 (C_{11}), 70.78 (C_7), 118.73 (C_5 and C_{15}), 120.95 (C_{13}), 122.65 (C_3), 126.87 (C_{18}), 127.19 (C_{25}), 127.85 (C_8), 128.38 (C_{24}), 128.67 (C_{19} and C_{23}), 128.87 (C_{20}), 137.13 (C_{14}), 138.25 (C_4), 138.88 (C_{22}), 139.32 (C_{17}), 150.81 (C_9), 154.19 (C_6), 156.65 (C_{16}), 159.14 (C_2 or C_{12}), 159.25 (C_2 or C_{12}), 185.74 (C_{10}). FT-IR (NaCl, cm^{-1}) 1688 and 1733 (C=O), 3465 (OH); HRMS (FAB^+) m/z = 488.1990; Calcd for $C_{32}H_{28}N_3O_3^+$ 488.1974. FT-IR (NaCl, cm^{-1}) 1671

(C=O), 3300 (OH); HRMS (FAB$^+$) m/z = 474.2175; Calcd for $C_{32}H_{28}N_3O_2^+$ 474.2182.

Catalytic Oxidation of Benzylamine with Cu^{II}4. Benzylamine (77 mg, 0.72 mmol) was added to an acetonitrile solution (5 mL) of **Cu^{II}4** (5 mg, 7.2 *m*mol) and the solution was stirred for 24 h at room temperature. After the reaction, the solvent was removed under reduced pressure to give a brown residue, which was then dissolved in CH_2Cl_2 (10 mL) and treated with a 25% NH_3 aqueous solution (5 mL). The aqueous solution was then extracted with CH_2Cl_2 (15 mL × 3), and the combined organic layer was dried over Na_2SO_4. After the removal of Na_2SO_4 by filtration, evaporation of the solvent gave a brown material, in which formation of *N*-benzylidene benzylamine was confirmed by ^{1}H NMR. Yield of the imine product was determined as 840%, based on **Cu^{II}4**, using $CHCl_2CHCl_2$ as an internal reference; turnover number of the catalyst is 8.4. ^{1}H NMR (300 MHz, $CDCl_3$): δ 4.83 (2 H, s, CH_2), 7.26−7.43 (8 H, m), 8.40 (1 H, s, CH); MS (FAB$^+$) m/z = 196.2; Calcd for $C_{32}H_{25}N_3O_3^+$ 196.1.

Computational Methods. All geometries were fully optimized at the M06-L level of density functional theory (DFT),[8] using the Stuttgart [8s7p6d | 6s5p3d] ECP10MWB contracted pseudopotential basis set on Cu[9] and the 6-31G(d) basis set[10] on all other atoms. In addition, three uncontracted f functions, having exponents of 5.100, 1.275, and 0.320, were placed on Cu. The grid = ultrafine option (in Gaussian 09[11]) was chosen for integral evaluation and an automatically generated density-fitting basis set was used within the resolution-of-the-identity approximation for the evaluation of Coulomb integrals. The nature of all stationary points was verified by analytic computation of vibrational frequencies, which were also used for the computation of zero-point vibrational energies, molecular partition functions (with all frequencies below 50 cm^{-1} replaced by 50 cm^{-1} when computing free energies), and for determining the reactants and products associated with each transition-state structure (by following the normal modes associated with imaginary frequencies). Partition functions were used in the computation of 298 K thermal contributions to free energy, employing the usual ideal-gas, rigid-rotator, harmonic oscillator approximation.[12] Solvation effects associated with methanol as a solvent were taken into account using the SMD continuum solvation model.[13]

The addition of triplet molecular oxygen to the doublet Cu(II) complexes may, in principle, generate either doublet or quartet products. Many of the doublet spin states were characterized by weak coupling between two different spin centers (the phenoxyl radical and a Cu(II) superoxide) and, therefore, are not well described by a single determinant nor appropriately treated by the standard Kohn−Sham density functional formalism. In this work, spin-purified doublet energies were computed relative to the quartet state through invocation of the standard Heisenberg−Dirac Hamiltonian[14] for two centers A and B, which has eigenvalues of

$$E_S = -J_{AB}S(S+1) \quad (1)$$

where J_{AB} is the coupling constant between the two centers, S takes on whole or half-integer values (ranging from $|S_A - S_B|$ to $|S_A + S_B|$), and $-S_A(S_A+1) - S_B(S_B+1)$ has been moved into the zero of energy. For the case where center A is a phenoxyl radical (S_A = 0.5) and center B is a triplet-coupled Cu(II)-superoxide (S_B = 1.0), S = 0.5 for the doublet state and S = 1.5 for the quartet state, such that

$$^DE = {}^QE + 3J_{AB} \quad (2)$$

We compute J_{AB} using the Yamaguchi equation:[15]

$$J_{AB} = -\frac{^{HS}E - {}^{BS}E}{^{HS}\langle S^2\rangle - {}^{BS}\langle S^2\rangle} \quad (3)$$

where ^{HS}E is the energy of the single-determinantal high-spin state at the low-spin geometry, ^{BS}E is the energy of the broken-symmetry low-spin state, and $\langle S^2\rangle$ is the expectation value of the total spin operator applied to the appropriate high-spin (HS) or broken-symmetry (BS) determinant.

To predict the NMR ^{1}H chemical shifts of possible products, structures were fully optimized at the M06-2X/6-31+G(d,p) level of theory,[16] taking into account solvation effects using the integral equation formalism[17] of the polarized continuum model[18] (IEFPCM) for chloroform as a solvent. The NMR shifts were calculated at the B3LYP/6-311+G(2d,p) level[19] with IEFPCM solvation. The molecular cavities for these calculations were constructed as a sum of atom-centered spheres, using the radii of Bondi.[20]

Results and Discussion

Synthesis. Ligands **L^mH** and **L^pH** were prepared by reductive coupling between compound **1** and compound **2^p** or **2^m**, using $NaBH_3CN$ as the reductant, followed by deprotection of the methoxy group using BBr_3 (see Scheme 2).

The copper(II) complexes **$Cu^{II}L^m$H** and **$Cu^{II}L^p$H** were prepared by treating the corresponding ligands with $Cu^{II}(ClO_4)_2\cdot 6H_2O$ in acetonitrile, and **$Cu^{II}L^o$** was synthesized as described in our previous study.[7] Figure 3 shows the crystal structures of **$Cu^{II}L^m$H** and **$Cu^{II}L^p$H**. The crystallographic data of the copper(II) complexes, together with selected bond lengths and angles, are summarized in Tables 1 and 2, respectively. The crystal structure of **$Cu^{II}L^o$** has already been reported in our previous

(8) Zhao, Y.; Truhlar, D. G. *J. Chem. Phys.* **2006**, *125*, 194101–194118.
(9) Dolg, M.; Wedig, U.; Stoll, H.; Preuss, H. *J. Chem. Phys.* **1987**, *86*, 866–872.
(10) Hehre, W. J.; Radom, L.; Schleyer, P. v. R.; Pople, J. A. *Ab Initio Molecular Orbital Theory*; Wiley: New York, 1986.
(11) Frisch, M. J.; Trucks, G. W.; Schlegel, H. B.; Scuseria, G. E.; Robb, M. A.; Cheeseman, J. R.; Scalmani, G.; Barone, V.; Mennucci, B.; Petersson, G. A.; Nakatsuji, H.; Caricato, M.; Li, X.; Hratchian, H. P.; Izmaylov, A. F.; Bloino, J.; Zheng, G.; Sonnenberg, J. L.; Hada, M.; Ehara, M.; Toyota, K.; Fukuda, R.; Hasegawa, J.; Ishida, M.; Nakajima, T.; Honda, Y.; Kitao, O.; Nakai, H.; Vreven, T.; Montgomery, J. A.; , Jr., Peralta, J. E.; Ogliaro, F.; Bearpark, M.; Heyd, J. J.; Brothers, E.; Kudin, K. N.; Staroverov, V. N.; Kobayashi, R.; Normand, J.; Raghavachari, K.; Rendell, A.; Burant, J. C.; Iyengar, S. S.; Tomasi, J.; Cossi, M.; Rega, N.; Millam, J. M.; Klene, M.; Knox, J. E.; Cross, J. B.; Bakken, V.; Adamo, C.; Jaramillo, J.; Gomperts, R.; Stratmann, R. E.; Yazyev, O.; Austin, A. J.; Cammi, R.; Pomelli, C.; Ochterski, J. W.; Martin, R. L.; Morokuma, K.; Zakrzewski, V. G.; Voth, G. A.; Salvador, P.; Dannenberg, J. J.; Dapprich, S.; Daniels, A. D.; Farkas, O.; Foresman, J. B.; Ortiz, J. V.; Cioslowski, J.; Fox, D. J. Gaussian 09, Revision A.02; Gaussian, Inc.: Wallingford, CT, 2009.
(12) Cramer, C. J. *Essentials of Computational Chemistry: Theories and Models*, 2nd ed.; John Wiley & Sons: Chichester, U.K., 2004.
(13) Marenich, A. V.; Cramer, C. J.; Truhlar, D. G. *J. Phys. Chem. B* **2009**, *113*, 6378–6396.
(14) (a) Heisenberg, W. Z. *Physik* **1928**, *49*, 619. (b) Cramer, C. J.; Truhlar, D. G. *Phys. Chem. Chem. Phys.* **2009**, *11*, 10757–10816.
(15) (a) Yamaguchi, K.; Jensen, F.; Dorigo, A.; Houk, K. N. *Chem. Phys. Lett.* **1988**, *149*, 537–542. (b) Soda, T.; Kitagawa, Y.; Onishi, T.; Takano, Y.; Shigeta, Y.; Nagao, H.; Yoshioka, Y.; Yamaguchi, K. *Chem. Phys. Lett.* **2000**, *319*, 223–230.
(16) Zhao, Y.; Truhlar, D. G. *Theor. Chem. Acc.* **2008**, *120*, 215–241.
(17) Cancès, E.; Mennucci, B.; Tomasi, J. *J. Chem. Phys.* **1997**, *107*, 3032–3041.
(18) Miertus, S.; Scrocco, E.; Tomasi, J. *Chem. Phys.* **1981**, *55*, 117–129.
(19) (a) Becke, A. D. *Phys. Rev. A* **1988**, *38*, 3098–3100. (b) Lee, C.; Yang, W.; Parr, R. G. *Phys. Rev. B* **1988**, *37*, 785–789. (c) Becke, A. D. *J. Chem. Phys.* **1993**, *98*, 5648–5652. (d) Stephens, P. J.; Devlin, F. J.; Chabalowski, C. F.; Frisch, M. J. *J. Phys. Chem.* **1994**, *98*, 11623–11627.
(20) Bondi, A. *J. Phys. Chem.* **1964**, *68*, 441–451.

Scheme 2

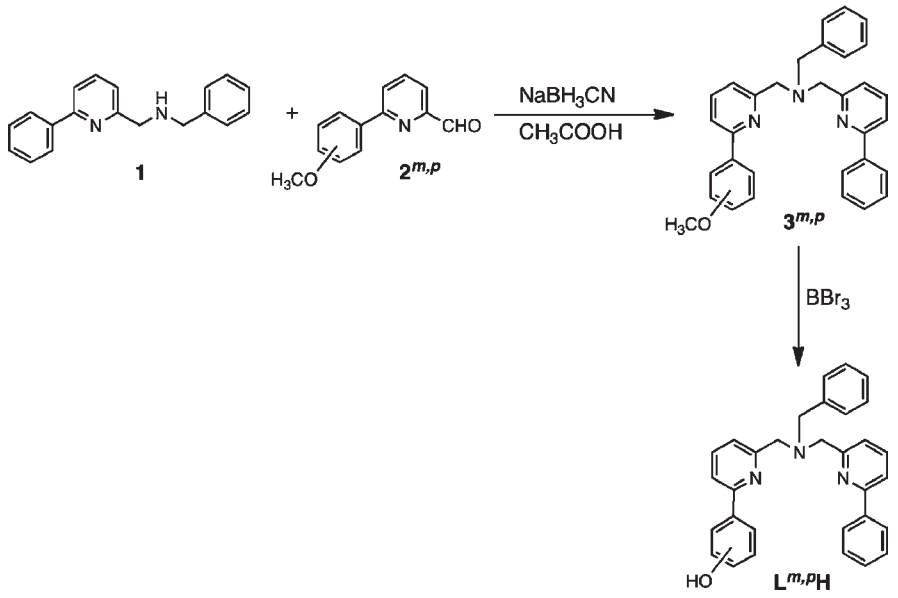

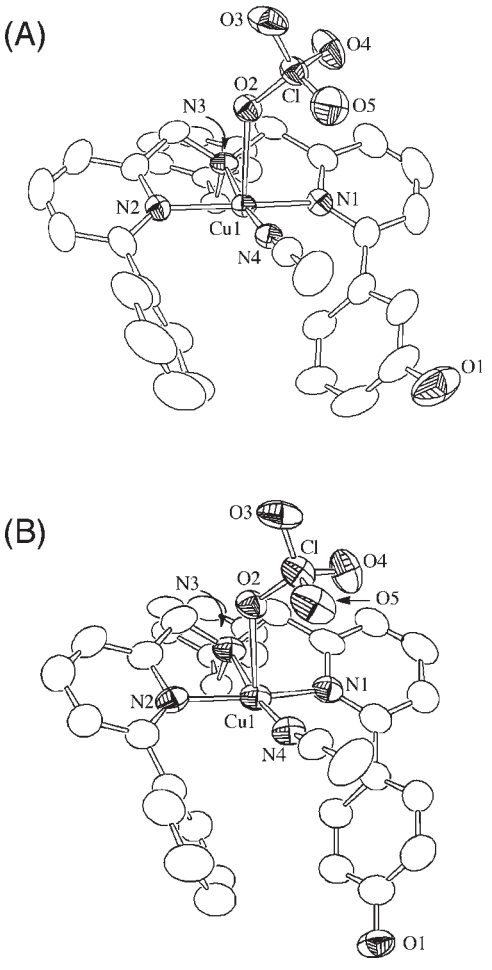

Figure 3. ORTEP drawings of (A) $Cu^{II}L^{m}H$ and (B) $Cu^{II}L^{p}H$ showing 50% probability thermal ellipsoids. Hydrogen atoms are omitted for clarity.

Communication, and it has direct coordination of the deprotonated phenolic oxygen to copper(II), as indicated in Chart 2.[7]

Table 1. Summary of the X-ray Crystallographic Data of $Cu^{II}L^{m}H$ and $Cu^{II}L^{p}H$

	$Cu^{II}L^{m}H$	$Cu^{II}L^{p}H$
formula	$C_{33}H_{30}N_4Cl_2O_9Cu$	$C_{33}H_{30}N_4Cl_2O_9Cu$
formula weight	761.07	761.07
crystal I	monoclinic	monoclinic
space group	$C2/c$ (#15)	$C2/c$ (#15)
a	28.313(11) Å	23.3974(11) Å
b	8.669(2) Å	16.2969(7) Å
c	29.689(11) Å	17.6996(9) Å
β	112.927(18)°	99.6154(5)°
V	6711(4) $Å^3$	6654.1(5) $Å^3$
Z	8	8
$F_{(000)}$	3128.00	3128.00
D_{calcd}	1.506 g/cm^3	1.591 g/cm^3
T	153 K	113 K
crystal size	0.40 mm × 0.10 mm × 0.10 mm	0.40 mm × 0.20 mm × 0.20 mm
μ(Mo Kα)	8.705 cm^{-1}	8.780 cm^{-1}
$2\theta_{max}$	55.0°	54.9°
no. of reflns measd	30720	31950
no. of reflns obsd	7649 ($[I > 2.00\sigma(I)]$)	7572 (all reflections)
no. of variables	479	498
$R1^a$	0.0470	0.0706
$wR2^b$	0.1264	0.2443
goodness of fit, GOF	0.912	0.977

$^a R1 = \sum||F_o| - |F_c||/\sum|F_o|$. $^b wR2 = [\sum(w(F_o^2 - F_c^2)^2/\sum F_o^2)^2]^{1/2}$.

Both $Cu^{II}L^{m}H$ and $Cu^{II}L^{p}H$ exhibit monomeric structures that have distorted square pyramidal structures, where the equatorial positions are occupied by the three nitrogen atoms N(1), N(2), N(3) from the ligand and an additional nitrogen atom from the external ligand CH_3CN; one of the oxygen atoms of the ClO_4 counteranion occupies the axial position. The τ values of $Cu^{II}L^{m}H$ and $Cu^{II}L^{p}H$ are 0.127 and 0.065, respectively.[21] Apparently, there is no direct interaction between the phenol group and the copper(II) ion in either complex, in contrast to the case of $Cu^{II}L^{o}$. In both $Cu^{II}L^{m}H$ and $Cu^{II}L^{p}H$, the phenol oxygen atoms are

(21) Addison, A. W.; Rao, T. N.; Reedijk, J.; van Rijn, J.; Verschoor, G. C. *J. Chem. Soc., Dalton Trans.* **1984**, 1349–1356.

Table 2. Selected Bond Lengths and Bond Angles of $Cu^{II}L^{m}H$ and $Cu^{II}L^{p}H$

Compound $Cu^{II}L^{m}H$			
Bond Lengths			
Cu(1)−N(1)	2.0230(17) Å	Cu(1)−N(2)	2.0267(16) Å
Cu(1)−N(3)	2.008(2) Å	Cu(1)−N(4)	1.962(2) Å
Cu(1)−O(2)	2.491(2) Å		
Bond Angles			
N(1)−Cu(1)−N(2)	161.86(9)°	N(1)−Cu(1)−N(3)	81.36(8)°
N(1)−Cu(1)−N(4)	97.26(8)°	N(2)−Cu(1)−N(3)	82.71(8)°
N(2)−Cu(1)−N(4)	99.98(8)°	N(3)−Cu(1)−N(4)	169.38(7)°
Compound $Cu^{II}L^{p}H$			
Bond Lengths			
Cu(1)−N(1)	2.020(4) Å	Cu(1)−N(2)	2.021(4) Å
Cu(1)−N(3)	2.008(3) Å	Cu(1)−N(4)	1.956(4) Å
Cu(1)−O(3)	2.510(3) Å		
Bond Angles			
N(1)−Cu(1)−N(2)	164.13(17)°	N(1)−Cu(1)−N(3)	82.14(17)°
N(1)−Cu(1)−N(4)	95.90(17)°	N(2)−Cu(1)−N(3)	83.31(16)°
N(2)−Cu(1)−N(4)	99.64(16)°	N(3)−Cu(1)−N(4)	168.02(16)°

Chart 2

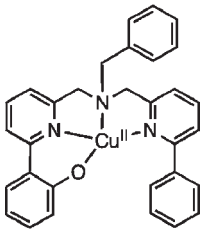

CuL^{o}

disordered, being found partially at both the *meta*- and *para*-positions of the phenyl groups of the ligand side arms.

ESR spectra of the copper(II) complexes have been measured in CH_3OH at 77 K, as shown in Figure S1 in the Supporting Information, and the ESR parameters of each complex are summarized in Table 3. Complex $Cu^{II}L^{o}$ exhibits a typical spectrum of copper(II) with a tetragonal geometry (see Figure S1A in the Supporting Information). Double integration of the ESR spectrum of $Cu^{II}L^{o}$ indicated that more than 95% spin persisted in solution, demonstrating a monomeric structure of $Cu^{II}L^{o}$ in solution. Notably, complexes $Cu^{II}L^{m}H$ and $Cu^{II}L^{p}H$ showed effectively identical ESR spectra with a relatively small $A_{//}$ value (107 G, as seen in Figures S1B and S1C in the Supporting Information). Thus, it can be said that the OH groups at the *meta*- and *para*-positions of the phenyl substituent in $Cu^{II}L^{m}H$ and $Cu^{II}L^{p}H$ do not interact with the copper(II) ion in solution, in agreement with what is seen in the crystal structures. The relatively small $A_{//}$ value of the complexes $Cu^{II}L^{m}H$ and $Cu^{II}L^{p}H$ suggests that the geometry of the complexes changes from distorted square pyramidal in the crystal to distorted trigonal bipyramidal in solution. Spin quantification of $Cu^{II}L^{m}H$ and $Cu^{II}L^{p}H$ also demonstrated that both complexes exist in a monomeric form in solution, again as in the case of the crystals.

Table 3. ESR Parameters of $Cu^{II}L^{o}$, $Cu^{II}L^{m}H$, and $Cu^{II}L^{p}H$[a]

	ESR Parameters		
complex	$g_{//}$	$g_{\perp}$	$A_{//}$
$Cu^{II}L^{o}$	2.231	2.056	174 G
$Cu^{II}L^{m}H$	2.429	2.093	107 G
$Cu^{II}L^{p}H$	2.429	2.093	107 G

[a] In CH_3OH at 77 K; microwave frequency = 9.03 GHz, modulation frequency = 100 kHz, modulation amplitude = 3 G, microwave power = 1.00 mW.

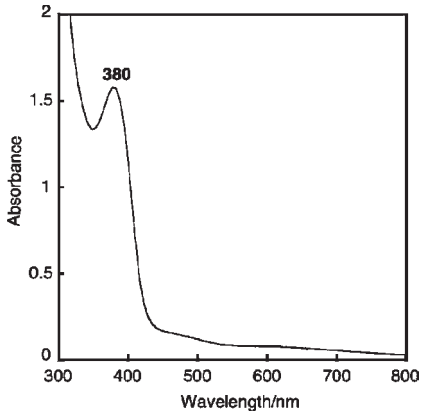

Figure 4. Ultraviolet−visible light (UV−vis) spectrum of $Cu^{II}L^{o}$ (0.5 mM) under O_2 atmosphere in methanol at 60 °C in a UV cell with a path length of 1.0 cm.

Reactivity of Copper(II) Complexes toward O_2. To examine the redox interaction between the copper(II) ion and the phenolate moiety of the ligand, the reactions of the copper(II) complexes and O_2 were studied in methanol in the presence of Et_3N as a base; in the case of $Cu^{II}L^{o}$, Et_3N was not added to the reaction solution, since, in that instance, the phenol proton of the ligand is already deprotonated in the starting complex.

O_2−Reactivity of $Cu^{II}L^{o}$. The copper(II) complex of L^{o-} ($Cu^{II}L^{o}$) exhibits an intense phenolate to copper(II) LMCT band at 380 nm (ε = 3650 M^{-1} cm^{-1}), together with a shoulder near 470 nm and a weak d−d band at 619 nm (ε = 140 M^{-1} cm^{-1}) in methanol under anaerobic conditions.[22] Introduction of O_2 into the solution hardly affected the spectrum at 60 °C for several hours, demonstrating that complex $Cu^{II}L^{o}$ was stable under an O_2 atmosphere (Figure 4). In the ESI-MS of the final reaction solution, there was a set of peaks at 519.4, corresponding to the starting material $[Cu^{II}(L^{o})]^{+}$ (calcd value: 519.1) after exposure to O_2. These results clearly indicate that this complex, with direct coordination of phenolate to copper(II), exhibits almost no reactivity toward molecular oxygen under the experimental conditions.

O_2−Reactivity of $Cu^{II}L^{m}H$. In contrast to the above *o*-phenol system $Cu^{II}L^{o}$, which does not show any reactivity toward O_2, treatment of $Cu^{II}L^{m}H$ in methanol with 2 equiv of Et_3N at 60 °C under an O_2 atmosphere gave a spectral change, as shown in Figure 5, where an intense absorption band at 410 nm and a weak broad band at 550−700 nm gradually appeared ($(8.7 \pm 0.9) \times 10^{-5}$ s^{-1}).

(22) (a) Jazdzewski, B. A.; Tolman, W. B. *Coord. Chem. Rev.* **2000**, *200−202*, 633–685. (b) Itoh, S.; Taki, M.; Fukuzumi, S. *Coord. Chem. Rev.* **2000**, *198*, 3–20.

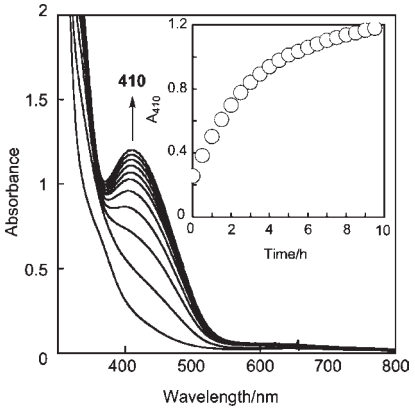

Figure 5. Spectral change of the aerobic reaction of $\mathbf{Cu^{II}L'''H}$ (0.5 mM) in methanol containing Et_3N (1.0 mM) at 60 °C in a UV cell with a path length of 1.0 cm. Inset: The time course of the absorption change at 410 nm.

Such a spectral change was not observed in the absence of O_2 (anaerobic conditions), clearly demonstrating that O_2 is required for the formation of the 410-nm chromophore. Also note that no distinct intermediate was observed during the course of the reaction, as seen in Figure 5. This may indicate that, in the presence of 2 equiv of Et_3N, the initial deprotonation step from the phenol moiety of $\mathbf{Cu^{II}L'''H}$ is the rate-limiting step in the overall reaction pathway, as discussed below (cf. Scheme 4).

The ESI-MS of the final reaction mixture shown in Figure 6 exhibits a set of peaks starting at 595.1 (Figure 6A), the mass number and isotope distribution pattern of which are identical to those of the simulation spectrum for a copper(II) complex containing modified ligand **4** (see Chart 3) and methoxide (OCH_3) (Figure 6C). Isotope labeling experiments using $^{18}O_2$ (purity 95%, Cambridge Isotope Laboratories, Inc.) gave the ESI-MS result shown in Figure 6B, where the main peak appeared at 597.0 (a two-mass-unit shift). This clearly demonstrates that one of the oxygen atoms incorporated into **4** originates from molecular oxygen. Computer simulation of the spectrum shown in Figure 6C (Figure 6D) indicates that the content of ^{18}O is 69%.

To confirm the structure of the modified ligand, the organic products were isolated by an ordinary workup of the final reaction mixture using aqueous NH_3 solution (demetallation) and subsequent chromatography on silica (see the Experimental Section). Two organic products, **4** and **5H**, were isolated and identified as indicated below.

Compound **4** exhibited m/z = 502.2159 in the HRMS analysis (calcd for $[\mathbf{4} + H]^+$, 502.2123), and two carbonyl C=O stretching vibration peaks at 1672 and 1727 cm^{-1} in the IR spectrum. In the ^1H NMR spectra of **4**, shown in Figure S2 in the Supporting Information, there is a sharp singlet at δ = 3.71 that has a peak area corresponding to the three protons of the methoxy group ($-OCH_3$). Another characteristic in the ^1H NMR is the existence of a doublet of doublets in an *ab* quartet pattern centered at δ = 6.75, which clearly indicates the existence of two olefinic protons strongly coupled to each other (see Figure S2 in the Supporting Information). Further structural information for **4** was obtained by NOE measurements, as indicated in Scheme 3. Irradiation of the methoxide peak at δ = 3.71 provided an NOE (1.3%) only on a peak at δ = 7.17, which is assigned as aromatic proton H^c on the pyridine nucleus (see Scheme 3 and Figure S3 in the Supporting Information). This confirms the close proximity of the methoxy proton ($-OCH_3$) and the pyridine nucleus, and it rules out an alternative structure **4′**, in which the $-OCH_3$ group and the olefinic proton H^b are sufficiently close that an NOE should be observed between them. In addition, irradiation of H^c at δ = 7.17 gave a NOE to the aromatic proton H^d on the pyridine nucleus at δ = 7.73 and the methoxy protons at δ = 3.71, but showed no NOE to the olefinic protons at δ = 6.75. This observation rules out structure **4″**, in which H^c and olefinic proton H^a should be close enough in some conformations to exhibit a NOE. Finally, the chemical shifts of H^a and H^b were estimated using ChemBioDraw Ultra (version 12.0); expert-system predictions are δ = 6.87 and 6.87 for **4**, 5.89 and 8.09 for **4′**, and 7.23 and 5.89 for **4″**. Obviously, the best match to the experimental data (δ = 6.75) is for **4**. Thus, the HRMS, IR, and ^1H NMR data, including NOE, support the *p*-quinone structure of **4**. The isolated compound **4** exhibited an absorption spectrum similar to the final spectrum shown in Figure 5, exhibiting an intense absorption band at ~410 nm and a weak broad band at 550−700 nm assignable to $\pi-\pi^*$ and $n-\pi^*$ transitions of the *p*-quinone moiety, respectively. The absorption spectrum resembles those of the TPQ cofactors,[1−3] further supporting formation of the *p*-quinone derivative **4**.

A second isolated product from chromatography, **5H**, exhibited m/z = 488.1990 in the HRMS analysis (calcd for $[\mathbf{5H} + H]^+$, 488.1896), and two carbonyl C=O stretching vibration peaks at 1686 and 1731 cm^{-1}, together with a broad intense absorption band at 3474 cm^{-1} due to the OH group in the IR spectrum. In the ^1H NMR shown in Figure S4 in the Supporting Information, the methoxy protons found in the spectrum of compound **4** are absent in **5H**. However, the two doublet peaks at δ = 6.71 and 6.83 indicate that the two olefinic protons on the modified ligand still remain. Furthermore, two carbonyl carbons are detected at 183.5 and 184.3 ppm in the ^{13}C NMR spectrum shown in Figure S5 in the Supporting Information. On the basis of these spectral data, together with the detailed 2D NMR analyses (HSQC, HH-COSY, and HMBC) shown in Figure S6 in the Supporting Information, the structure of compound **5H** has been secured and all the ^1H and ^{13}C NMR peaks have been completely assigned, as indicated in the insets of Figures S4 and S5 in the Supporting Information. Since compound **5H** was not contained in the crude reaction mixture prior to SiO_2 column chromatography (as judged by ^1H NMR), compound **5H** must be generated from compound **4** during chromatography.[23]

A possible mechanism for the formation of $\mathbf{Cu^{II}4}$ from $\mathbf{Cu^{II}L'''H}$ is presented in Scheme 4. Treatment of $\mathbf{Cu^{II}4}$ with triethylamine (2 equiv) in methanol may induce deprotonation of methanol and the phenolic proton of the ligand to give, after coordination of methoxide,

(23) The NMR data of compound **5H** are slightly different from those of essentially the same compound (L2H) reported in our previous Communication (ref 6e). Detailed analysis of the FAB-MS data of the present compound (**5H**) indicated that there is a small peak at 504.2, which corresponds to a molecular mass of [**5H** + H_2O]. Thus, in the present compound, **5H** may bind one molecule of H_2O in the ligand cavity, which influences the NMR chemical shifts of the compound.

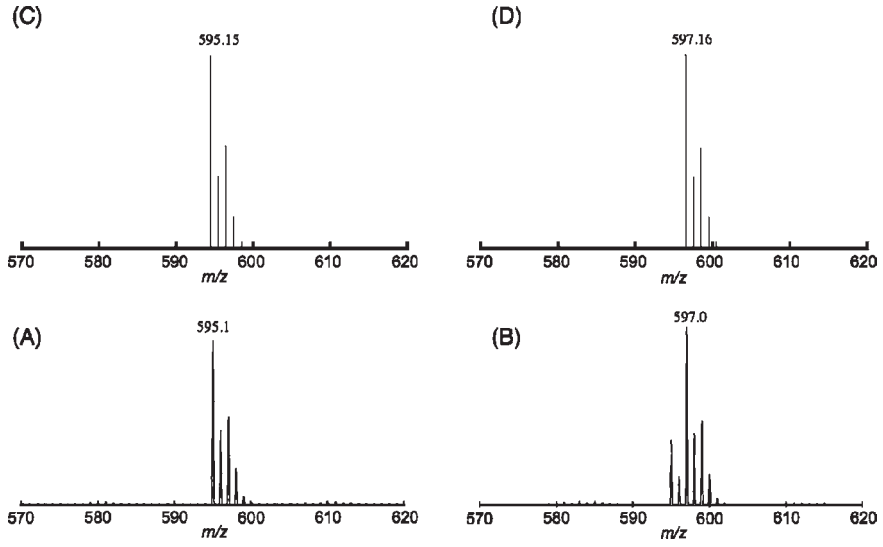

Figure 6. ESI−MS spectra of (A) $[Cu^{II}(\mathbf{4})(OCH_3)]^+$ ($\mathbf{Cu^{II}4}$) generated using $^{16}O_2$ and (B) $[Cu^{II}(\mathbf{4})(OCH_3)]^+$ ($\mathbf{Cu^{II}4}$) generated using $^{18}O_2$. Simulated spectra of these products are shown in panels C and D, respectively.

Scheme 3

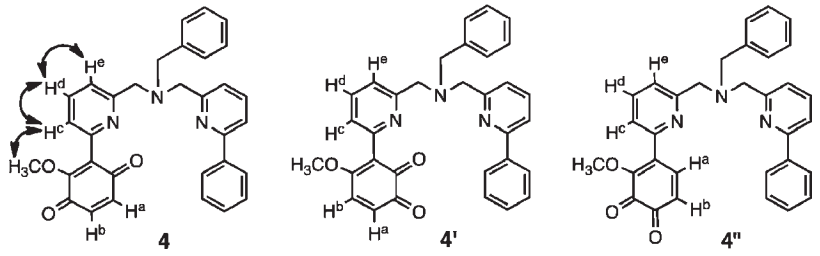

Scheme 4

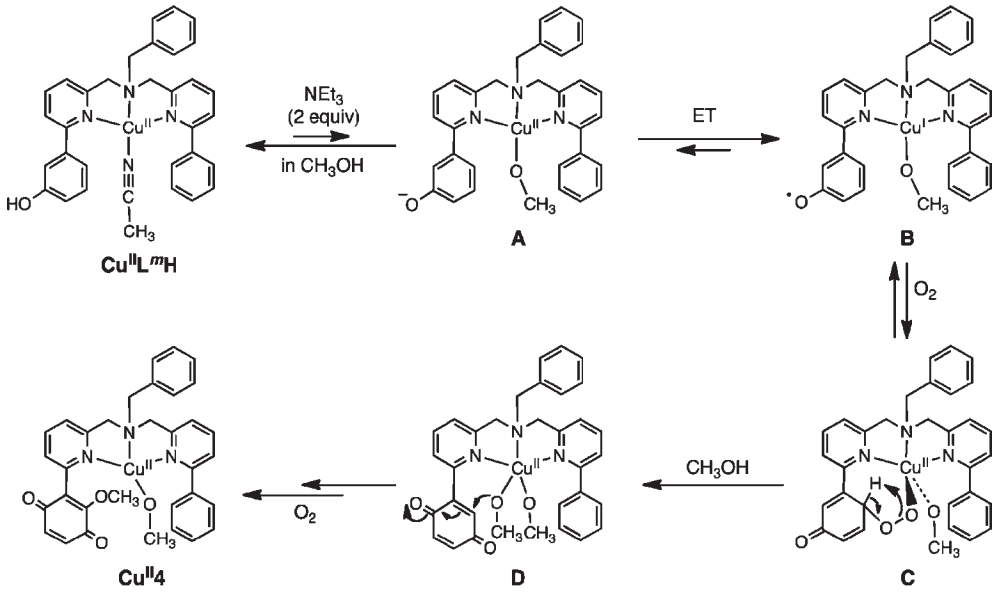

intermediate **A**. Either concomitantly or subsequently, intramolecular electron transfer from the generated phenolate moiety to copper(II) ion may occur to generate a copper(I)-phenoxyl radical species **B**, to which molecular oxygen may be added to generate an alkylperoxo-type intermediate **C**, where the peroxide group bridges the *para*-position of the aromatic substituent and the copper ion. Heterolytic cleavage of the O−O bond in **C** generates *p*-quinone intermediate **D**. In subsequent steps, Michael addition of methoxide and aerobic oxidation of the reduced quinone occur, to deliver the final product $\mathbf{Cu^{II}4}$.

To gain further insight into the precise mechanistic pathway and the nature of the various potential intermediates, density functional theory (DFT) calculations

Chart 3

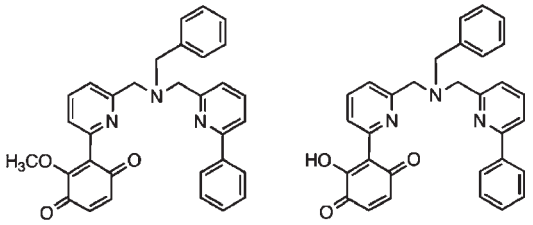

4 **5H**

were undertaken (see the above Computational Methods section for full details). To begin, the uncharged molecule with a deprotonated phenol and a methoxide ligand coordinated to the copper atom was chosen. Because of the distorted tetragonal coordination of the copper atom and the asymmetry of the phenol group, several conformational isomers were considered and four distinct structures were found as local minima, differing in (a) the absolute configuration of the benzyl-substituted nitrogen atom (which will readily invert at experimental temperatures) and (b) the rotational orientation of the phenol group; these conformers had relative free energies of 0.0, 0.2, 6.8, and 7.8 kcal/mol (all free energies presented in this discussion include the effects of continuum methanol solvation). While all structures and energies are provided in the Supporting Information, in the interests of brevity, here, we will focus our discussion on the theoretical results for the lowest-energy species; the lowest-energy conformer $\mathbf{i_B}$ may be found in Figure 7. [For discussion of the microscopic mechanism, we have adopted lowercase roman numerals for the individual intermediates and transition-state (TS) structures. In cases where those structures correspond to species in Scheme 4, we add, as a subscript, the capital letter corresponding to the labeling in Scheme 4. Thus, for example, $\mathbf{i_B}$ indicates the correspondence between optimized intermediate **i** and structure **B**.]

The electronic structure of intermediate $\mathbf{i_B}$, which has a doublet spin state, is best described as a Cu(I) complex with the unpaired spin density located primarily on the phenoxyl fragment; in particular, the spin densities on the O, C(2), C(4), and C(6) positions of the phenoxyl ring (taking C(3) as the position of substitution of the attached pyridine) were computed to be 0.22, 0.17, 0.18, and 0.14 a.u., respectively. That is, DFT predicts the ground electronic state of this complex to correspond to **B** in Scheme 4. In this respect, structure **A** in Scheme 4 is formally an excited electronic state, relative to **B**. To better understand the nature of the complex *immediately* after the deprotonation step, and to further illuminate the relationship between **A** and **B** (Scheme 4), complex **i** was also optimized in the presence of the ammonium ion generated directly from deprotonation of the phenol (including methanol continuum solvation). Population analysis clearly shows that, in the presence of the ammonium ion, the ground-state electronic structure of the tight ion pair is best represented by **A** in Scheme 4—the unpaired spin is essentially entirely found in a Cu d orbital. TDDFT calculations indicate that the lowest-energy electronic transition in the tight ion pair is indeed that corresponding to intramolecular electron transfer to generate **B**. Computation of the rate of reaction for **A** going to **B** is beyond the scope of the present study, because the complex dynamics of electron transfer and tight ion-pair dissociation in a polar solvent are both involved and could likely be addressed only by explicit quantum mechanical simulations. Nevertheless, it is apparent that both of the two diabatic states represented by structures **A** and **B** in Scheme 4 are energetically accessible under the experimental conditions.

It may be that deprotonation of the phenol moiety of $\mathbf{Cu^{II}L'''H}$ to give **A** is the rate-determining step in the presence of a small amount of the base (2 equiv of Et_3N) in the overall reaction pathway, as mentioned previously. If the deprotonation step were fast enough to generate a sufficient amount of phenolate **A**, a copper(I)−phenoxyl radical species (intermediate **B**) should be detected in the initial stage of the reaction. However, the formation of such an organic radical species could not be detected by ESR and UV−vis. When a large excess of Et_3N (< 100 equiv) was added to enhance the deprotonation step, a complicated mixture of oligomeric products was obtained. This may be due to the C−C coupling reactions of the phenoxyl radical intermediate **B** generated in solution. Thus, to suppress such an undesirable side reaction (C−C coupling reaction), the addition of a limited amount of Et_3N (2 equiv) was necessary (see Figure 5).

Next, we examined the coordination of molecular oxygen to the copper atom. We successfully located four low- to moderate-energy conformational isomers for each of the doublet and quartet electronic states that may be generated by the addition of triplet molecular oxygen to doublet **B**. The lowest-energy such structure, quartet **ii**, is shown in Figure 7 (see also Figure 8 for a traditional reaction coordinate diagram, but bearing in mind that each intermediate and TS structure is more properly viewed as a population of related but different stereostructures, so that a single reaction coordinate curve, as opposed to a family of many such curves, is somewhat of a simplification). Structure **ii** is predicted to have a free energy of 2.9 kcal/mol, relative to infinitely separated $\mathbf{i_B}$ and molecular O_2; the other quartet conformers have free energies ranging from 3.3 kcal/mol to 8.0 kcal/mol. The doublet conformers are structurally quite similar to the quartet conformers and are predicted to have free energies that are ~4.8−9.6 kcal/mol, relative to infinitely separated $\mathbf{i_B}$ and molecular O_2. Within the accuracy of our DFT model, the two electronic states may be considered to be degenerate, which is consistent with very weak coupling between what spin density calculations indicate to be a phenoxyl radical and a triplet end-on Cu(II)-superoxide complex. The triplet end-on Cu(II)-superoxide character of the CuO_2 fragment is consistent with expectations, given the nature of the supporting ligands coordinated to the metal atom.[24]

Following characterization of the stable oxygen adducts, we proceeded to optimize TS structures for the addition of the distal oxygen of the O_2 fragment to the phenoxyl ring. We found 12 such structures, differing in conformation and the position of attack on the phenoxyl

(24) (a) Cramer, C. J.; Tolman, W. B. *Acc. Chem. Res.* **2007**, *40*, 601–608. (b) Cramer, C. J.; Gour, J. R.; Kinal, A.; Wtoch, M.; Piecuch, P.; Moughal Shahi, A. R.; Gagliardi, L. *J. Phys. Chem. A* **2008**, *112*, 3754–3767.

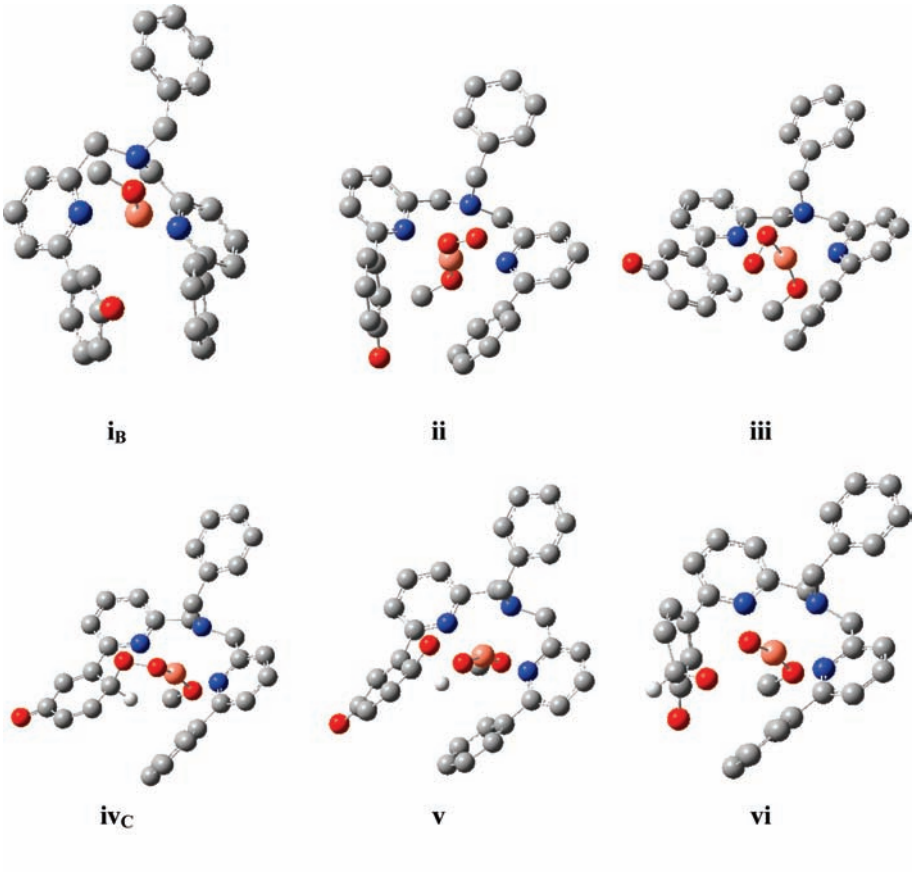

Figure 7. Ball-and-stick stereostructures for selected stationary points on the mechanistic pathway leading to **4**, as computed at the M06-L level of theory. For clarity, hydrogen atoms are not shown, except at the substituted aromatic position after electrophilic attack by oxygen. Hydrogen atoms are white, carbon atoms are gray, nitrogen atoms are blue, oxygen atoms are red, and copper atoms are latte.

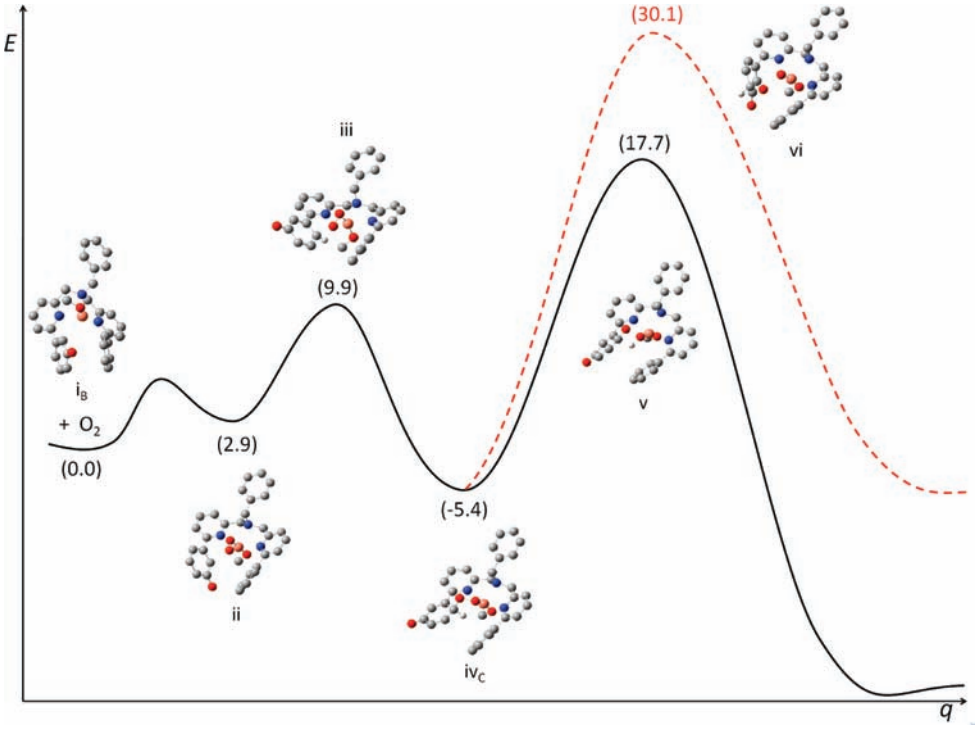

Figure 8. Reaction coordinate diagram for steps along the path from $\mathbf{i_B}$ to phenol ring oxygenation. Density functional theory (DFT) energies, including continuum solvation, are indicated in units of kcal/mol; see Figure 7 for larger structural images.

Scheme 5

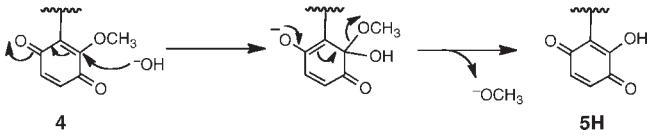

ring. All TS structures were predicted to have doublet spin states, which is consistent with the coupling of two spins in the forming C−O bond and dominant Cu(II) character, as illustrated for intermediate **C** in Scheme 4. Generally, we found additions to C(6) to be least favored, locating 4 structures with activation free energies, relative to separated $\mathbf{i_B}$ and O_2, ranging from 13.0 kcal/mol to 27.6 kcal/mol, and additions to C(2) and C(4) to be roughly equally favorable, with 4 structures in each case having activation free energies of 9.2−17.0 kcal/mol in the case of C(2) and 9.1−15.4 kcal/mol in the case of C(4). One such TS structure, **iii**, is shown in Figure 7; addition to C(4) has an activation free energy of 9.9 kcal/mol.

The intermediates that result from C−O bond formation (i.e., those structures analogous to **C** in Scheme 4) were computed to have free energies, relative to separated $\mathbf{i_B}$ and O_2, ranging from −5.4 kcal/mol to 13.5 kcal/mol. The largest free energy of activation for the *reverse* reaction from any adduct (i.e., breaking the newly formed C−O bond) is 15.3 kcal/mol, which corresponds to the reverse reaction of intermediate $\mathbf{iv_C}$, which is the lowest-energy adduct (Figure 7), passing back through structure **iii**.

The next step in the microscopic mechanism that we considered was scission of the O−O bond. For 9 of the 12 intermediates, we successfully located TS structures for this bond breakage. The TS structures fell into two classes, differing in the magnitude of the predicted activation free energies. In the lower-energy class, the geometry of the adduct permits a hydrogen-atom transfer from the newly oxygenated position to the departing oxygen atom at the same time that O−O bond breaking is taking place. That is, the direct product of the reaction is a quinone and a Cu(II) hydroxide (analogous to structure **D** in Scheme 4). In the higher-energy class, such a concerted hydrogen-atom transfer is geometrically impossible, and the resulting product is instead a high-energy species containing a copper-oxo fragment and an open-shell monohydrogenated quinone. The TS structures that we were unsuccessful in locating all corresponded to structures that would fall into the latter, high-energy class, and they are presumably not readily located, because of the high energy of the resulting products. Figure 7 illustrates one TS structure from each class: **v** (leading to copper hydroxo) and **vi** (leading to copper oxo).

In the case of the lower-energy class of TS structures, bond scission for a C(2) adduct, to generate an *ortho*-quinone, is predicted to have an activation free energy (again, relative to infinitely separated $\mathbf{i_B}$ and O_2) of 15.6 kcal/mol, and an analogous TS structure for a C(4) adduct (**v**), to generate a *para*-quinone, is predicted to have an activation free energy of 17.7 kcal/mol. Within the accuracy of the model, these two pathways are predicted to be about equally likely. Activation free energies for all other TS structures for this step range from 22.5 kcal/mol to 36.1 kcal/mol. The larger activation free energy in every case for O−O bond breaking, compared to C−O bond formation, indicates that it is the O−O scission step that is product-determining in the phenol oxygenation process, so that the relative stabilities of the preceding intermediates and the ease of their formation does not dictate the final position of oxygenation. Theory does not address whether this step is also *rate*-determining, because the activation free energies of the (possibly coupled) deprotonation and electron-transfer steps leading to $\mathbf{i_B}$ have not been quantified.

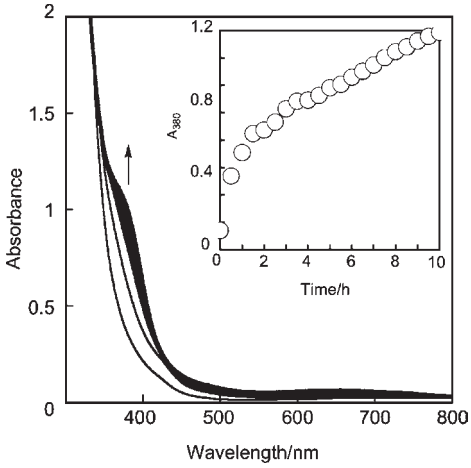

Figure 9. Spectral change for the aerobic reaction of $\mathbf{Cu^{II}L^{\prime}H}$ (0.5 mM) in methanol containing Et_3N (1.0 mM) at 60 °C in a UV cell with a path length of 1.0 cm. Inset shows the time course of the absorption change at 380 nm.

The remaining steps in the proposed mechanism—namely, Michael addition to the quinone and subsequent oxidation of the product—were not assessed with DFT. The observation of **4** as a product and not **4′** is not entirely consistent with the theoretical prediction that TS structures leading to the precursor *para*- and *ortho*-quinones, respectively, have roughly equal activation free energies. However, mass recovery of crude **4** is only 51% (vide supra), so this discrepancy may reflect instability of the missing isomer to subsequent reaction or workup conditions.

With respect to the assignment of the structure of compound **5H**, we also computed the ^{1}H chemical shifts for geometries of **5H** and **5H″** (the latter being the hydroxy analogue of **4″** shown in Scheme 3; **5H′**, the corresponding analog of **4′**, was not considered, because it is a tautomer of **5H** and would be expected to readily equilibrate). The B3LYP/6-311+G(2d,p)//M06−2X/6-31+G(d,p) predictions for the olefinic protons in **5H** are 6.63 and 6.76 ppm, which is in near-quantitative agreement with the experimental values of 6.71 and 6.83. The predicted shifts for **5H″**, on the other hand, are 5.92 and 8.20 ppm. These data provide further confirmation for the structural assignment of **5H**. As noted previously, compound **5H** is likely generated from compound **4** via a SiO_2-assisted hydrolysis of the methoxy group during the column chromatographic treatment of compound **4** (see Scheme 5).

O_2 Reactivity of $\mathbf{Cu^{II}L^{\prime}H}$. Complex $\mathbf{Cu^{II}L^{\prime}H}$ also reacted in methanol at 60 °C in the presence of NEt_3 (2 equiv), as shown in Figure 9. Although the time course of the absorption change is not simple (see inset of Figure 9),

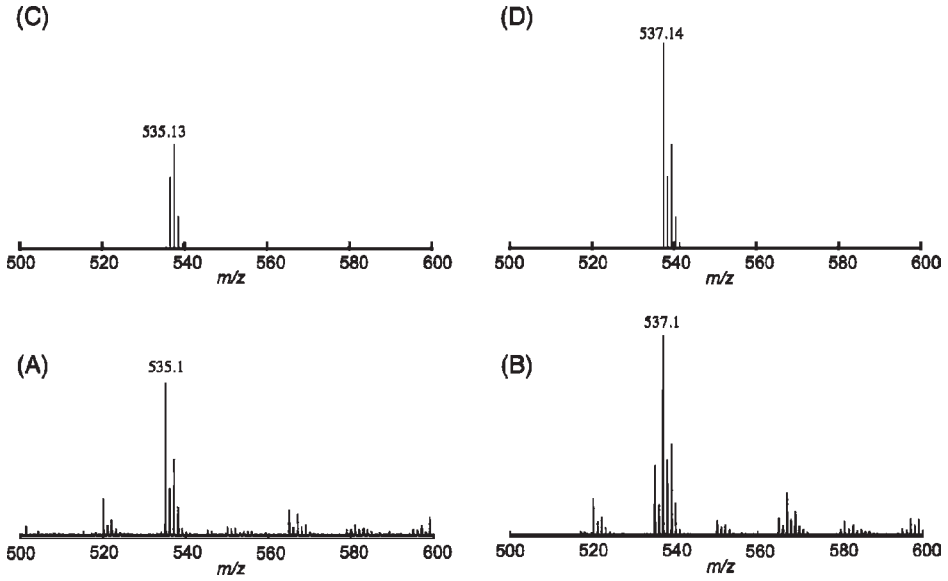

Figure 10. ESI−MS spectra of (A) $[Cu^{II}(\mathbf{6})]^+$ ($\mathbf{Cu^{II}6}$) generated using $^{16}O_2$ and (B) $[Cu^{II}(\mathbf{6})]^+$ ($\mathbf{Cu^{II}6}$) generated using $^{18}O_2$. Simulated spectra of these products are shown in panels C and D, respectively.

the absorption band at ~380 nm gradually increases. In this case as well, no spectral change was observed in the absence of O_2 (anaerobic conditions), demonstrating that O_2 is involved in the reaction as a substrate. The ESI-MS spectrum shown in Figure 10A exhibits a set of peaks starting at 535.1, which clearly indicates incorporation of one oxygen atom into the product (see Figure 10C, calcd value: 535.13). Isotope labeling experiment using $^{18}O_2$ (purity 95%, Cambridge Isotope Laboratories, Inc.) gave an ESI-MS shown in Figure 10B, where the main peak appears at 537.1 (a two mass unit shift). This clearly demonstrates that one of the oxygen atoms incorporated into **6** also originates from molecular oxygen. Computer simulation of the spectrum shown in Figure 10C (Figure 10D) indicates that the content of ^{18}O is 70%.

The organic product **6H** was isolated by ordinary demetallation of the product complex using NH_4OH and subsequent SiO_2 column chromatography, as in the former reaction. In the ^1H NMR spectrum shown in Figure S7 in the Supporting Information, there are two doublet peaks at $\delta = 6.26$ and 6.72, which couple to each other with a coupling constant $J = 8.8$ Hz. Judging from the integral ratio of these doublets, each peak involves two protons. Furthermore, a singlet peak at 6.48 disappears when D_2O is added to the ^1H NMR sample, indicating that this peak is due to an acidic (easily exchanged) proton, such as an OH proton. In the ^{13}C NMR shown in Figure S8 in the Supporting Information, there is only one peak at 185.9, which is ascribable to a carbonyl carbon. Furthermore, in the IR spectrum, there is an intense peak at 1671 cm^{-1}, which is ascribable to a C=O stretching vibration, and a broad OH absorption peak at 3300 cm^{-1}. On the basis of these spectral data, together with the detailed 2D NMR analyses (HSQC, HH-COSY, and HMBC) shown in Figure S9 in the Supporting Information, the structure of organic product **6H** has been assigned as the keto-alcohol derivative shown in Chart 4, and all the ^1H and ^{13}C NMR peaks have been completely assigned as indicated in Figures S7 and S8 in the Supporting Information, respectively.

Chart 4

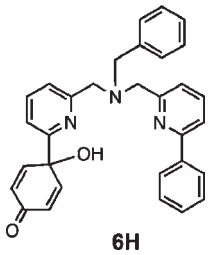

6H

A possible mechanism for the formation of complex $\mathbf{Cu^{II}6}$ from $\mathbf{Cu^{II}L^{\mathit{p}}H}$ is shown in Scheme 6.

Deprotonation of $\mathbf{Cu^{II}L^{\mathit{p}}H}$ produces $\mathbf{Cu^{II}L^{\mathit{p}}}$ (**A** in Scheme 6), within which intramolecular electron transfer occurs from the generated phenolate moiety to the copper(II) ion to provide intermediate **B**. Next, molecular oxygen adds to **B** to generate an alkylperoxo-type intermediate **C**, where the peroxide group bridges the C_7 *ipso* carbon of the phenol ring and the copper ion. Electronically, both C_7 and C_9 might be expected to be available for formation of the peroxide bridge with the copper(II) ion, but only product from the C_7 adduct is isolated. Ultimately, oxidation of the coordinated methoxide by the generated peroxide may occur to give $\mathbf{Cu^{II}6}$ and formaldehyde (HCHO). In this case as well, the deprotonation step from $\mathbf{Cu^{II}L^{\mathit{p}}H}$ may be the rate-limiting process, since no distinct intermediate was detected in the UV−vis spectrum (see Figure 9); however, the mechanistic details of this process have yet to be established.

Catalytic Oxidation of Benzylamine. The catalytic oxidation of benzylamine was briefly examined using the quinone complexes $\mathbf{Cu^{II}4}$ in acetonitrile at room temperature (see Scheme 7). *N*-Benzylidene benzylamine was obtained as the oxidation product in 840% yield, based on the quinone catalyst (i.e., multiple turnovers are observed; turnover number of the catalyst is 8.4). Thus, the quinone−copper(II) complexes generated from the phenol derivatives actually act as turnover catalysts for amine oxidation. Although the mechanistic details have yet to be

Scheme 6

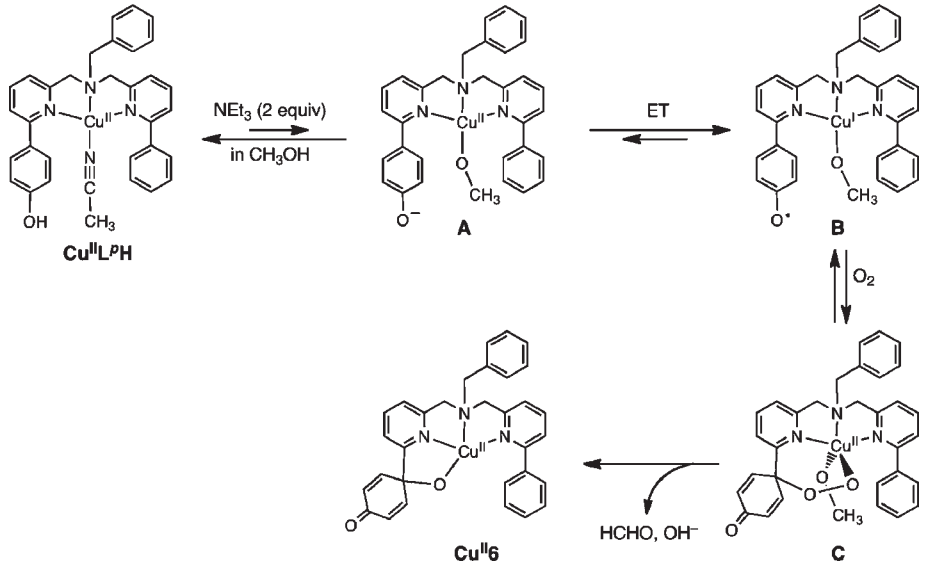

Scheme 7

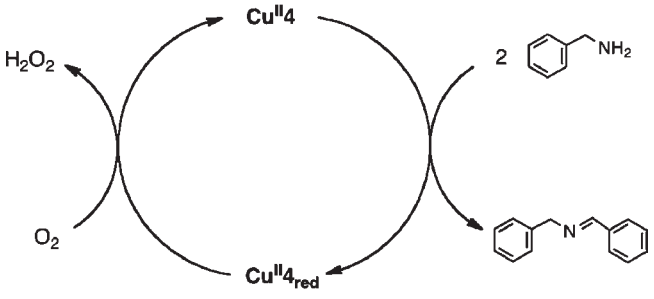

examined in detail, the reaction may involve a *trans-amination* mechanism, as suggested for amine oxidation by the model compounds of cofactors TPQ, PQQ (pyrroloquinolinequinone), and TTQ (tryptophan tryptophylquinone).[25]

Summary

In this study, copper(II) complexes supported by a series of redox active phenol ligands $\mathbf{L^oH}$, $\mathbf{L^{m}H}$, and $\mathbf{L^pH}$ (shown in Chart 1) have been synthesized, and their O_2 reactivity has been explored in detail, to gain mechanistic insights into the biosynthetic processes that lead to the novel organic TPQ cofactor (2,4,5-trihydroxyphenylalanine quinone, TOPA quinone) in copper-containing amine oxidases.

The copper(II)-phenolate complex $\mathbf{Cu^{II}L^o}$ (*ortho*-phenol derivative) involves a strong coordination of the phenolate oxygen to copper(II) (Cu−O distance is 1.891 Å),[7] and it is stable under O_2 in CH_3OH at 60 °C (essentially no change was observed after several hours). On the other hand, the copper(II)−phenol complex $\mathbf{Cu^{II}L^{m}H}$ (*meta*-phenol derivative) reacts with O_2 in the presence of triethylamine as a base in CH_3OH at 60 °C to give a methoxy-substituted *para*-quinone derivative (compound **4**; see Chart 3). The structure of the product has been established through detailed nuclear magnetic resonance (NMR) analyses, electrospray ionization−mass spectroscopy (ESI-MS) (including an ^{18}O-labeling experiment), and infrared (IR) spectroscopy. The density functional theory (DFT) calculations are consistent with a mechanistic pathway that begins with an exergonic intramolecular electron transfer from the deprotonated phenol (phenolate) to copper(II) in **A** (shown in Scheme 4), to generate a copper(I)−phenoxyl radical species **B**. Molecular oxygen is added to **B** to form an end-on superoxo copper(II) species **ii**, shown in Figure 7, from which C−O bond formation through electrophilic attack on the aromatic ring occurs to give a copper(II)−alkylperoxo type intermediate **C**. From this intermediate, O−O bond cleavage and proton migration proceeds in a concerted manner to provide a *para*-quinone derivative **D**. DFT suggests that a stepwise O−O bond cleavage to generate a formal Cu(III)−oxo species, followed by subsequent proton migration, is energetically much less favorable in the reaction pathway from **A** to **D** (see Figure 8). The final step is Michael addition of a methoxide on the copper(II) ion to the *para*-quinone ring and subsequent O_2 oxidation. These reaction steps are very close to those proposed for the biosynthesis of TPQ cofactor in the enzymatic system shown in Scheme 1. Thus, the present reaction can be regarded as a good model for TPQ biosynthesis, providing important insights into the nature of postulated intermediates.

However, there is a critical difference between our model reaction and the enzymatic reaction. Namely, under our present reaction conditions, using a small amount of triethylamine base (2 equiv), deprotonation from the phenol moiety of $\mathbf{Cu^{II}L^{m}H}$ is rate-limiting in regard to the overall reaction pathway. Thus, once the phenolate is generated from the neutral phenol by deprotonation, the subsequent reactions (electron transfer, generating intermediate **B**; O_2 addition to make alkylperoxide derivative **C**; O−O bond cleavage to give the *p*-quinone derivative **D**; and Michael addition of methanol to form the final product) may proceed smoothly. Thus, any intermediates were not detected in our model system (see Figure 5). If an excess amount of the base (< 100 equiv) was added to the methanol solution of $\mathbf{Cu^{II}L^{m}H}$, a complicated mixture of oligomeric products was obtained. This may be

(25) (a) Mure, M.; Klinman, J. P. *J. Am. Chem. Soc.* **1995**, *117*, 8698–8706. (b) Itoh, S.; Mure, M.; Ogino, M.; Ohshiro, Y. *J. Org. Chem.* **1991**, *56*, 6857–6865. (c) Itoh, S.; Takada, N.; Haranou, S.; Ando, T.; Komatsu, M.; Ohshiro, Y.; Fukuzumi, S. *J. Org. Chem.* **1996**, *61*, 8967–8974.

due to the C−C coupling reaction of the phenoxyl radical intermediate **B**, which is generated in a relatively large amount in solution in the presence of a large excess of Et_3N. Thus, the TPQ formation is only observed successfully in the presence of a limited amount of ET_3N, where the copper(I) phenoxyl radical species exists as a very minor component, to prevent the C−C coupling reaction. In the enzyme active site, such a C−C coupling reaction does not proceed at all, so that one can detect the intermediates. This is a limitation of model studies. Nevertheless, the generated *para*-quinone derivative can act as a turnover catalyst for aerobic oxidation of benzylamine to *N*-benzylidene benzylamine, as shown in Scheme 7. The reaction may involve a *trans-amination* mechanism, as in the cases of other quinone cofactor model compounds.[25]

When the position of the phenolic OH group was changed from *meta* to *para*, relative to the pyridine donor group in copper(II)-phenol complex $\mathbf{Cu^{II}L^{\mathit{p}}H}$, the oxygenation reaction involved electrophilic substitution at the *ipso*-position, to give a keto-alcohol derivative **6H** (see Chart 4). The structure of this oxygenated product is fundamentally different from that of the TPQ cofactor. Thus, the present results strongly suggest that the steric relation between the copper(II) ion and the phenol moiety of the reactive tyrosine residue is critically important for its conversion to the TPQ cofactor in the enzyme active site. Furthermore, the poor O_2 reactivity of $\mathbf{Cu^{II}L^{\mathit{o}}}$ may suggest that such strong coordination of phenolate to copper(II) is not favorable for the reaction with O_2. This is consistent with the observation that the coordinative interaction between the copper(II) ion and the unmodified tyrosine precursor is fairly weak in the initial stage of TPQ biosynthesis: the Cu−O distance is ∼2.5 Å,[1j] which is much larger than that in $\mathbf{Cu^{II}L^{\mathit{o}}}$ (1.891 Å).[7,26]

(26) The optimized structure for the $\mathbf{Cu^{II}L^{\mathit{m}}H}$ shows a distance of 4.351 Å between the oxygen atom of the phenolate and the Cu^{II} ion, which is much longer that the distance between the copper ion and thyrosyl oxygen in the enzyme active site (2.57 Å). However, through-bond electron transfer from the phenolate ring to copper(II) could be possible in the model system, because the phenol ring is covalently connected to the pyridine donor group that is directly coordinated to copper(II).

Acknowledgment. S.I. acknowledges the financial support by Grant-in-Aid for Science Research on Priority Areas (No. 200360044, Synergy of Elements; No. 21108515, π-Space) from Ministry of Education, Culture, Sports, Science and Technology, Japan and also by the Asahi Glass Foundation and the Mitsubishi Foundation. We also thank Dr. Kyoko Inoue of the Analytical Center of Osaka University for her assistance in obtaining the 2D NMR data. C.J.C. and M.Z.E. thank the U.S. National Science Foundation for support (through Grant Nos. CHE-0610183 and CHE-0956776).

Supporting Information Available: Further details are given in Figures S1−S19 (PDF), Table S1 (PDF), and in a CIF file. This material is available free of charge via the Internet at http://pubs.acs.org.